
ASYMMETRIC HUBER PERIODOGRAM

Tianbo Chen¹

¹School of Big Data and Statistics, Anhui University, China, Email: chentianbo@ahu.edu.cn

ABSTRACT

This paper introduces a novel spectral M-estimator, called the asymmetric Huber periodogram (AHP), for periodicity detection in time series. The AHP is constructed from trigonometric asymmetric Huber regression, where a specially designed check function is used to substitute the squared ℓ_2 norm that defines the ordinary periodogram (PG). The AHP is statistically more efficient than the quantile periodogram (QP), while offering a more comprehensive picture than the Huber periodogram (HP) by examining the data across the entire range of the asymmetric parameter. We prove the theoretical properties of the AHP and investigate the relationship between the AHP and the so-called asymmetric Huber spectrum (AHS). Finally, simulations and three real-world data examples demonstrate that the AHP's capability in detecting periodicity and its robustness against outliers.

Keywords: Asymmetric Huber regression; Periodicity detection; Periodogram; Robustness; Spectral analysis.

1 Introduction

The PG, a raw non-parametric estimator of the power spectrum, plays a crucial role in spectral analysis and is widely applied across various fields (Caiado et al., 2006; Polat and Güneş, 2007; Baud et al., 2018; Euán et al., 2018; Maadooliat et al., 2018; Martínez-Murcia et al., 2019; Chen et al., 2021a). The PG is constructed by trigonometric ordinary least squares (OLS) regression. However, OLS exhibits limitations in terms of robustness and efficiency, particularly in handling data with asymmetric or heavy-tailed distributions. Moreover, OLS regression focuses on the conditional mean, lacking the ability to provide a complete picture of the distribution of the data, which subsequently affects the performance of the PG (Bloomfield, 2004). As a result, alternative regression techniques have been proposed to overcome the issues of OLS.

The pioneering work of Koenker and Bassett Jr (1978) introduced the concept of quantile regression (QR). By substituting the ℓ_2 loss with asymmetric ℓ_1 loss, QR provides a more complete picture of the relationship between

the response variable and the covariates across different quantile levels, while also demonstrating strong robustness against outliers and heavy-tailed distributions. For a detailed and systematic introduction to quantile regression and its extensions, we refer to Kouretas et al. (2005); Cai and Xu (2008); Cai and Xiao (2012); Koenker (2017). However, QR is not free of limitations: the non-smooth check (loss) function causes both theoretical and computational burdens, and it suffers efficiency losses under Gaussian or homoscedastic errors. Based on this, asymmetric least squares (ALS) regression, also known as expectile regression (ER), was proposed by Newey and Powell (1987). The quadratic form of the loss function partly addresses the limitations inherent in QR, but this improvement comes at the expense of a certain degree of robustness. A comprehensive comparative analysis of quantiles and expectiles is presented in Waltrup et al. (2015), wherein the relationships between these two approaches are thoroughly examined. Further theoretical analysis between QR and ER can be found in Efron (1991); Jones (1994); Yao and Tong (1996). Because of their advantages, QR and ER, as well as their extensions, have been widely used across various scientific fields (Garcia et al., 2001; Machado and Mata, 2005; Gu and Zou, 2016; Ziegel, 2016; Bellini and Di Bernardino, 2017; Jiang et al., 2017; Daouia et al., 2018; Xu et al., 2020; Alvarado et al., 2021; Sharif et al., 2021; Xu et al., 2021). As a generalization of both QR and ER, Jiang et al. (2021) introduced the k -th power expectile regression (KER) with $1 < k \leq 2$.

With these regression techniques, researches have developed the corresponding periodograms. One innovative development is the QP (Li, 2012b) constructed by trigonometric QR, which demonstrates its ability to detect hidden periodicities in time series. Similar to ordinary spectral analysis, large-sample analysis reveals that the QP is associated with the so called quantile spectrum, which is a scaled version of the ordinary power spectrum of the level-crossing process. The Laplace periodogram (LP) is a special case of the QP by setting the quantile to 0.5. Related works on the QP include Li (2012a); Hagemann (2013); Li (2014); Dette et al. (2015); Kley (2016); Birr et al. (2017); Meziari et al. (2020); Chen et al. (2021b); Li (2023). Chen (2024) further proposed the EP, and comprehensively compared it with the QP. For more robust periodograms, Wen et al. (2021) proposed the HP and Thieler et al. (2016) developed the R package RobPer, which allows users to combine different regression techniques (Rousseeuw and Yohai, 1984; Oh et al., 2004; Ahdesmäki et al., 2007; Thieler, 2014) to calculate robust periodograms.

Besides KER, the asymmetric Huber regression (AHR) (Allende et al., 2006) also strikes a balance between robustness and efficiency using piecewise linear and quadratic losses, with a threshold parameter to control the ratio of the two losses. In addition to the original Huber loss (Huber, 1964), the AHR uses an asymmetric parameter that similar to quantile and expectile, to comprehensively analyze the distribution of the data. In this paper, we apply asymmetric Huber trigonometric regression and propose a spectral estimator called AHP. We demonstrate that the AHP not only shares similar properties with the PG, LP, and HP as a frequency-domain representation of serial dependence in time series, but also provides a more comprehensive analysis by exploring the data across different asymmetric parameters.

The remainder of the paper is organized as follows. We first introduce the AHP in Section 2. The large sample theory revealing the asymptotic distribution of the AHP, which is presented in Section 3. In Section 4, we present comparative studies evaluating the performance of different types of periodograms by simulation studies. In Section 5, we apply

the AHP to three real data examples, demonstrating its ability to detect hidden periodicities and its robustness against outliers. Finally, we conclude the paper and list the limitations and possible future work in Section 6.

2 Asymmetric Huber Periodogram

Suppose that $\{y_t\}$ is a stationary process with distribution function $F(\cdot)$. For any fixed asymmetric parameter $\alpha \in (0, 1)$ and threshold parameter $\psi > 0$, define the asymmetric Huber loss¹ as

$$\rho_{\alpha, \psi}(u) = \begin{cases} |\alpha - I(u < 0)| \cdot \frac{1}{2}u^2, & |u| \leq \psi, \\ |\alpha - I(u < 0)| \cdot \psi(|u| - \frac{1}{2}\psi), & |u| > \psi. \end{cases}$$

In the special case of $\psi \rightarrow 0$ and $\psi \rightarrow \infty$, the loss function reduces to the check loss function of quantile regression and the asymmetric quadratic loss function of expectile regression, respectively. The α -th asymmetric Huber quantile (AHQ) of y_t is defined as

$$\mu(\alpha, \psi) := \arg \min_{\mu \in \mathbb{R}} \mathbb{E} \{ \rho_{\alpha, \psi}(y_t - \mu) \}, \quad (1)$$

with the normal equation

$$\mathbb{E} \{ \dot{\rho}_{\alpha, \psi}(y_t - \mu(\alpha, \psi)) \} = 0. \quad (2)$$

Given a time series $\{y_t : t = 1, \dots, n\}$ and regressors $\mathbf{x}_{nt}(\omega_\nu) := [\cos(\omega_\nu t), \sin(\omega_\nu t)]^\top$, the AHR solves the optimization problem:

$$\hat{\boldsymbol{\beta}}_n(\alpha, \psi) := \arg \min_{\boldsymbol{\beta} \in \mathbb{R}^2} \sum_{t=1}^n \rho_{\alpha, \psi}(y_t - \mu - \mathbf{x}_{nt}^\top \boldsymbol{\beta}), \quad (3)$$

where ω_ν denotes the Fourier frequencies in $(0, \pi)$, $\hat{\boldsymbol{\beta}}_n(\omega_\nu, \alpha, \psi) := [\hat{\beta}_1(\omega_\nu, \alpha, \psi), \hat{\beta}_2(\omega_\nu, \alpha, \psi)]^\top$, and μ is a suitable constant, typically the sample α -th AHQ of y_t . Then, the Asymmetric Huber discrete Fourier transform (AHDFT) of $\{y_t : t = 1, \dots, n\}$ at level α is defined as

$$z_n(\omega_\nu, \alpha, \psi) := \frac{n}{2} \{ \hat{\beta}_1(\omega_\nu, \alpha, \psi) - i \hat{\beta}_2(\omega_\nu, \alpha, \psi) \},$$

where $i := \sqrt{-1}$. The AHDFT can be viewed as an extension of the ordinary DFT, which is defined as

$$z_n(\omega_\nu) := \sum_{t=1}^n y_t \exp(-i\omega_\nu t).$$

When $\alpha = 0.5$ and $\psi \rightarrow \infty$, the AHDFT coincides with the ordinary DFT. With the AHDFT, the AHP is defined as

$$\text{AHP}_n(\omega_\nu, \alpha, \psi) := n^{-1} |z_n(\omega_\nu, \alpha, \psi)|^2. \quad (4)$$

Below are some special cases of the AHP:

- Huber periodogram (Wen et al., 2021), when $\alpha = 0.5$,

¹Note that some literature, such as Gupta et al. (2020) and Hazarika et al. (2023), uses a different version, in which the loss function is symmetric when $|u| \leq \psi$.

- Ordinary periodogram, when $\alpha = 0.5, \psi \rightarrow \infty$,
- Expectile periodogram (Chen, 2024), when $\psi \rightarrow \infty$,
- Laplace periodogram (Li, 2008), when $\alpha = 0.5, \psi = 0$,
- Quantile periodogram (Li, 2012b), when $\psi = 0$.

Remark:

- In Sections 4 and 5, we only focus on serial dependence in time series, and the amplitude is considered secondary. As a result, we normalize the periodograms so that the summation over ω equals 1 for each pair (α, ψ) . Additionally, we use the normalized frequency $f = \omega/2\pi$, which represents the number of cycles per unit time, in all figures.

3 Asymptotic Analysis

In this section, we follow some key results in Jiang et al. (2021) to develop the large-sample asymptotic analysis, which reveals an association between the AHP and the so-called AHS.

For fixed α and ψ , let $\{y_t\}$ be a stationary process with cumulative distribution function $F(\cdot)$. We consider the joint asymptotic distribution of the AHP ordinates computed at q distinct frequencies, denoted by $\{\omega_{\nu_j} : j = 1, \dots, q\}$. Let $\mathbf{x}_{jnt} = [1, \cos(\omega_{\nu_j} t), \sin(\omega_{\nu_j} t)]^\top, t = 1, \dots, n, j = 1, \dots, q$. Substituting \mathbf{x}_{nt} with \mathbf{x}_{jnt} in (3), we obtain $\widehat{\beta}_{jn}(\alpha, \psi)$, and $\text{AHP}_n(\omega_{\nu_j}, \alpha, \psi)$. We define

$$\zeta_{jn}(\alpha, \psi) := n^{-1/2} \sum_{t=1}^n \dot{\rho}_{\alpha, \psi}(y_t - \mu(\alpha, \psi)) \mathbf{x}_{jnt}, \quad (5)$$

where

$$\dot{\rho}_{\alpha, \psi}(y_t - \mu(\alpha, \psi)) = \begin{cases} (\alpha - I(u < 0)) u, & |u| \leq \psi, \\ (\alpha - I(u < 0)) \psi \operatorname{sgn}(u), & |u| > \psi. \end{cases} \quad (6)$$

Let the following conditions be satisfied for fixed α and ψ :

- C1. $f(u) = \dot{F}(u)$ exists for all u and $F(u + \mu(\alpha, \psi)) - F(\mu(\alpha, \psi)) = f(\mu(\alpha, \psi))u + O(u^{d+1})$ uniformly for all $|u| \leq u_0$, where $d > 0$ and $u > 0$ are some constants.
- C2. The process $\{y_t\}$ has the strong mixing property with mixing numbers a_τ ($\tau = 1, 2, \dots$) satisfying $a_\tau \rightarrow 0$ as $\tau \rightarrow \infty$.
- C3. The process $\{\dot{\rho}_{\alpha, \psi}(y_t - \mu(\alpha, \psi))\}$ is stationary with zero mean and absolutely summable ACF defined as $\operatorname{Cov}\{\dot{\rho}_{\alpha, \psi}(y_t - \mu(\alpha, \psi)), \dot{\rho}_{\alpha, \psi}(y_s - \mu(\alpha, \psi))\} = \gamma(t-s, \alpha, \psi)$. And the distribution of $\{\dot{\rho}_{\alpha, \psi}(y_t - \mu(\alpha, \psi))\}$ has a continuous density around $\pm\psi$ for each j .

C4. A central limit theorem is valid for $\text{vec}[\zeta_{jn}(\alpha, \psi)]_{j=1}^q$ for all j , i.e., $\text{vec}[\zeta_{jn}(\alpha, \psi)]_{j=1}^q \xrightarrow{D} N(\mathbf{0}, [\mathbf{V}_{jl}(\alpha, \psi)]_{j,l=1}^q)$ as $n \rightarrow \infty$, where $\mathbf{V}_{jl}(\alpha, \psi)$ is the asymptotic covariance matrix of $\zeta_{jn}(\alpha, \psi)$ and $\zeta_{ln}(\alpha, \psi)$.²

By C3, we define

$$g(\omega, \alpha, \psi) = \eta^2(\alpha, \psi)h(\omega, \alpha, \psi), \quad (7)$$

where

$$h(\omega, \alpha, \psi) := \sum_{\tau=-\infty}^{\infty} \gamma(\tau, \alpha, \psi) \exp(-i\omega\tau) = \sum_{\tau=-\infty}^{\infty} \gamma(\tau, \alpha, \psi) \cos(\omega\tau). \quad (8)$$

The second expression in (8) follows from the symmetry $\gamma(\tau, \alpha, \psi) = \gamma(-\tau, \alpha, \psi)$. Suppose that $\Pr\{|y_t - \mu(\alpha, \psi)| < \psi\} = c > 0$, which leads to $E\{\ddot{\rho}(y_t - \mu(\alpha, \psi))\} \neq 0$. Then, the scaling factor $\eta(\alpha, \psi)$ is defined as

$$\begin{aligned} \eta^{-1}(\alpha, \psi) &= E\{\ddot{\rho}_{\alpha, \psi}(y_t - \mu(\alpha, \psi))\} \\ &= \alpha \Pr(0 < y_t - \mu(\alpha, \psi) < \psi) + (1 - \alpha) \Pr(-\psi < y_t - \mu(\alpha, \psi) < 0) \\ &= \alpha\{F(\psi + \mu(\alpha, \psi)) - F(\mu(\alpha, \psi))\} + (1 - \alpha)\{F(\mu(\alpha, \psi)) - F(\mu(\alpha, \psi) - \psi)\}, \end{aligned}$$

which depends solely on the marginal distribution $F(\cdot)$, where the derivative $\ddot{\rho}_{\alpha, \psi}(u) = \partial^2 \dot{\rho}_{\alpha, \psi}(u) / \partial u^2$ exists almost everywhere and is given by

$$\ddot{\rho}_{\alpha, \psi}(u) = \begin{cases} \alpha, & 0 < u < \psi, \\ \alpha - 1, & -\psi < u < 0, \\ 0, & |u| > \psi. \end{cases} \quad (9)$$

The non-differentiability at the kink points has no effect on the expectation, as it occurs with zero probability bases on (C3).

Equipped with these concepts, we establish the following theorem regarding the $\text{AHP}_n(\omega_{\nu_j}, \alpha, \psi)$ in (4).

Theorem 1. For fixed $q > 1$ and $0 < \lambda_1 < \dots < \lambda_q < \pi$, let $\omega_{\nu_1}, \dots, \omega_{\nu_q}$ be Fourier frequencies satisfying $\omega_{\nu_j} \rightarrow \lambda_j$ as $n \rightarrow \infty$ for $j = 1, \dots, q$. If (C1)–(C4) hold, then

$$\{\text{AHP}_n(\omega_{\nu_1}, \alpha, \psi), \dots, \text{AHP}_n(\omega_{\nu_q}, \alpha, \psi)\} \xrightarrow{D} \{g(\lambda_1, \alpha, \psi)(1/2)\chi_{2,1}^2, \dots, g(\lambda_q, \alpha, \psi)(1/2)\chi_{2,q}^2\}, \quad (10)$$

where $\chi_{2,1}^2, \dots, \chi_{2,q}^2$ are independent standard chi-square random variables with two degrees of freedom and \xrightarrow{D} denotes converge in distribution.

Proof. See Appendix. □

Theorem 1 shows that the AHP exhibits a scaled chi-square distributions with two degrees of freedom, similar to the behavior of the PG (Brockwell and Davis, 1991). The definition of $h(\omega, \alpha, \psi)$ in (8) can be extended to all $\omega \in [0, 2\pi)$, and it is nothing but the ordinary spectrum of the stationary process $\{\dot{\rho}_{\alpha, \psi}(y_t - \mu(\alpha, \psi))\}$. This process is

²This is a relaxed condition, see Remark 1 in Li (2012b) and Condition C3 in Chen (2024) for details.

just an asymmetrically-scaled version of the process $\{y_t - \mu(\alpha, \psi)\}$ around $\mu(\alpha, \psi)$. Similarly, as a scaled version of $h(\omega, \alpha, \psi)$, the definition of $g(\omega, \alpha, \psi)$ can also be extended to include all $\omega \in [0, 2\pi)$, which we define as the AHS of $\{y_t\}$.

4 Simulation Studies

In this section, we present experiments to evaluate the efficiency of the AHP in detecting hidden periodicities and its robustness against outliers, along with comparisons to other types of periodograms.

4.1 Hidden Periodicities Detection

Suppose that $\{x_t\}$ is an AR(2) model:

$$x_t = \phi_1 x_{t-1} + \phi_2 x_{t-2} + \epsilon_t, \quad (11)$$

which represents the case without hidden periodicities, and

$$y_t = (b_0 + b_1 \cos(\omega_{\nu_0} t) + b_2 \sin(\omega_{\nu_1} t))x_t, \quad (12)$$

which represents the case with hidden periodicities at $\omega_{\nu_0} = 0.09 \times 2\pi$ and $\omega_{\nu_1} = 0.12 \times 2\pi$. We set $b_0 = 1, b_1 = 0.9, b_2 = 1, \phi_1 = 2r \cos(\omega_{\nu_c}), \phi_2 = -r^2$ ($r = 0.6$), and $\{\epsilon_t\}$ is the standard Gaussian white noise. We first present the averaged periodograms from 5,000 simulation of model (11) with PG, LP, and HP as comparisons. As shown in Figure 1 (a) and (b), all types of periodograms exhibit similar bell-shaped patterns, with maximum value at $\omega_{\nu_c} = 0.25 \times 2\pi$. These results can be directly explained by the ordinary spectral analysis. Specifically, the characteristic polynomial of model (11) is $\phi(z) = 1 - \phi_1 z - \phi_2 z^2$, where the roots z_1 and z_2 are complex conjugates. The AR coefficients ϕ_1 and ϕ_2 determine the location of the spectral peak:

$$\omega = \arccos \frac{\phi_1}{2\sqrt{-\phi_2}} = \omega_{\nu_c},$$

and as $r \rightarrow 1^-$, the peak becomes sharper.

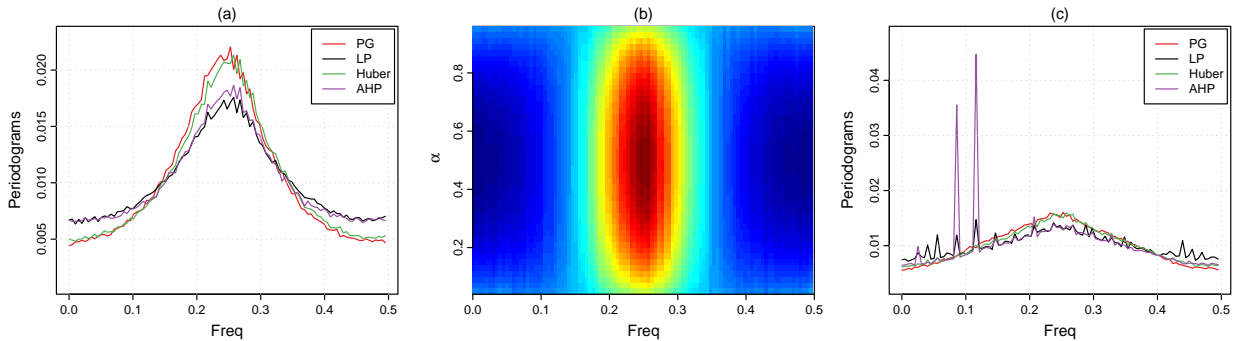


Figure 1: Left: averaged smoothed PG, LP, and AHP ($\alpha = 0.8, \psi = 1.345\hat{\sigma}_{x_t}$) of model (11). Middle: averaged smoothed AHP ($\alpha = 0.05, 0.07, \dots, 0.95, \psi = 1.345\hat{\sigma}_{x_t}$) of model (11). Right: PG, LP, and AHP ($\alpha = 0.8$ and $\psi = 1.345\hat{\sigma}_{y_t}$) of model (12). The number of realizations is 5,000 and the sample size is $n = 200$. The value 1.345 is suggested by Huber (1964).

The results of model (12), as illustrated by Figure 1 (c), the AHP successfully detects the hidden periodicities, resulting in large spikes at $\omega_{\nu_0} = 0.09 \times 2\pi$ and $\omega_{\nu_1} = 0.12 \times 2\pi$, whereas other types of periodograms do not exhibit this capability, producing similar bell-shaped patterns in model (11). We observe small spikes at some other frequencies in the LP, which caused by spectral leakages. This phenomenon is explained by Theorem 5 in Li (2008) and Theorem 2 in Li (2012b), and can also occur in the AHP.

The AHPs of many time series models, such as AR, ARIMA, and GARCH models, are symmetric across α (e.g., Figures 1 (b) and 5). To demonstrate the capability of the AHP in addressing more complex spectral features, we construct a nonlinear mixture model $\{y_t\}$, whose AHP is intentionally designed to be asymmetric across α :

$$y_t = W_2(z_t) z_t + \{1 - W_2(z_t)\} x_{t,3}, \quad (13)$$

where

$$z_t = W_1(x_{t,1}) x_{t,1} + \{1 - W_1(x_{t,1})\} x_{t,2}.$$

The components $\{x_{t,1}\}$, $\{x_{t,2}\}$, and $\{x_{t,3}\}$ are independent Gaussian AR processes given by $x_{t,1} = 0.8x_{t-1,1} + w_{t,1}$, $x_{t,2} = -0.75x_{t-1,2} + w_{t,2}$, and $x_{t,3} = -0.81x_{t-2,3} + w_{t,3}$, where $w_{t,1}, w_{t,2}, w_{t,3}$ are standard Gaussian white noise. From the perspective of traditional spectral analysis, the series $\{x_{t,1}\}$ has a lowpass spectrum, $\{x_{t,2}\}$ has a highpass spectrum, and $\{x_{t,3}\}$ has a bandpass spectrum around frequency $0.25 \times 2\pi$. The mixing function $W_1(x)$ and $W_2(x)$ are defined as

$$W_1(x) = \begin{cases} 0.75, & x < -0.8, \\ -\frac{13}{32}x + 0.425, & -0.8 \leq x \leq 0.8, \\ 0.1, & x > 0.8, \end{cases} \quad \text{and} \quad W_2(x) = \begin{cases} 0.5, & x < -0.4, \\ -1.25x, & -0.4 \leq x \leq 0, \\ 0, & x > 0. \end{cases}$$

Figure 2 shows the averaged smoothed periodograms of model (13) from 5,000 simulations, illustrating that the PG, LP, and HP are limited to capturing spectral features near the central quantile ($\alpha = 0.5$). In contrast, the AHP offers a broader perspective, effectively analyzing the time series across the entire range of $\alpha \in (0, 1)$.

4.2 Robustness Evaluation using Fisher's Test

In ordinary spectral analysis, Fisher's test (Brockwell and Davis, 1991) is applied to detect periodicities in the PG. For frequencies $\{\omega_{\nu_1}, \omega_{\nu_2}, \dots, \omega_{\nu_q}\}$, the test statistic is defined as

$$g = \frac{\max_{1 \leq j \leq q} \{I_n(\omega_{\nu_j})\}}{\sum_{j=1}^q I_n(\omega_{\nu_j})}.$$

The null hypothesis is that the time series is Gaussian white noise, while the alternative hypothesis is that the time series contains a deterministic periodic component of unspecified frequency. extend Fisher's test to the AHP by replacing $I_n(\omega)$ with $AHP_n(\omega, \alpha, \psi)$ in the test statistic.

Suppose that $\{y_t\}$ is an AR(2) process with

$$y_t = 0.9y_{t-1} - 0.9y_{t-2} + \epsilon_t, \quad (14)$$

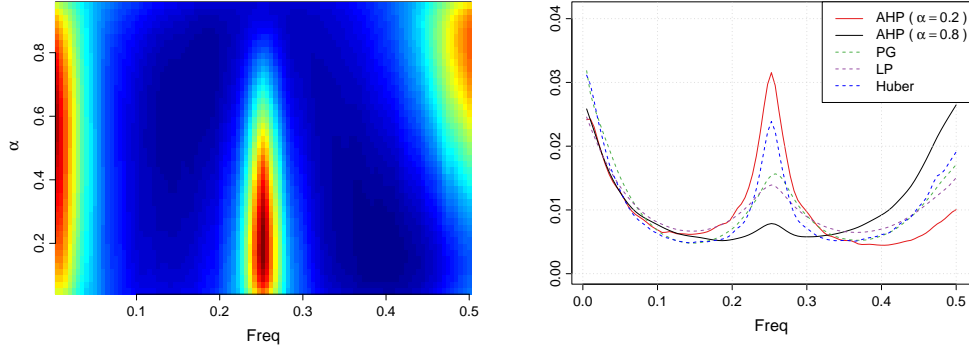


Figure 2: Left: AHP ($\alpha = 0.05, 0.07, \dots, 0.95$ and $\psi = 1.345\hat{\sigma}_{y_t}$). Right: AHP ($\alpha = 0.2, 0.8$ and $\psi = 1.345\hat{\sigma}_{y_t}$), LP, QP, and HP. Results are based on the average of 5,000 smoothed periodograms to generate the results, and the sample size $n = 200$. The smoothing uses `smooth.spline` function in R.

which has a single spectral peak at $0.171 \times 2\pi$. To evaluate the robustness of the AHP, we introduce three contamination models:

- Type 1 (single-point outlier): add a constant with magnitude c_1 to $\{y_t\}$ at a single time point t^* :

$$y_{1,t} = \begin{cases} y_t & \text{if } t \neq t^*, \\ y_t + c_1 & \text{if } t = t^*, \end{cases} \quad (15)$$

where t^* denote a random integer in $[1, n]$.

- Type 2 (short-term burst): add a peak with magnitude c_2 to $\{y_t\}$ at the interval $[t^*, t^* + 5]$:

$$y_{2,t} = \begin{cases} y_t & \text{if } t \notin [t^*, t^* + 5], \\ y_t + c_2 & \text{if } t \in [t^*, t^* + 5], \end{cases} \quad (16)$$

where t^* denote a random integer in $[1, n - 5]$.

- Type 3 (eyeblink artifact): eyeblink artifact is added to simulate contamination commonly observed in EEG data (Mansor et al., 2011; Abo-Zahhad et al., 2015; Chen, 2025): $\{y_t\}$:

$$y_{3,t} = \begin{cases} y_t & \text{if } t \notin [t^*, t^* + 50], \\ y_t + \text{eyebk}(t, c_3) & \text{if } t \in [t^*, t^* + 50], \end{cases} \quad (17)$$

where $\text{eyebk}(t)$ is the eyeblink artifact generated by two Gamma functions with eye-closure magnitude c_3 and eye-open magnitude $0.6c_3$, where t^* denote a random integer in $[1, n - 50]$.

Figure 3 shows the three types of outliers.

We generate 1,000 time series based on models (14) - (17), respectively, and compute their AHP, EP, and PG. In this experiment, we set $\alpha = 0.6, 0.8$, and the threshold parameter ψ is set to $(0.674, 0.935, 1.345)$ times the sample

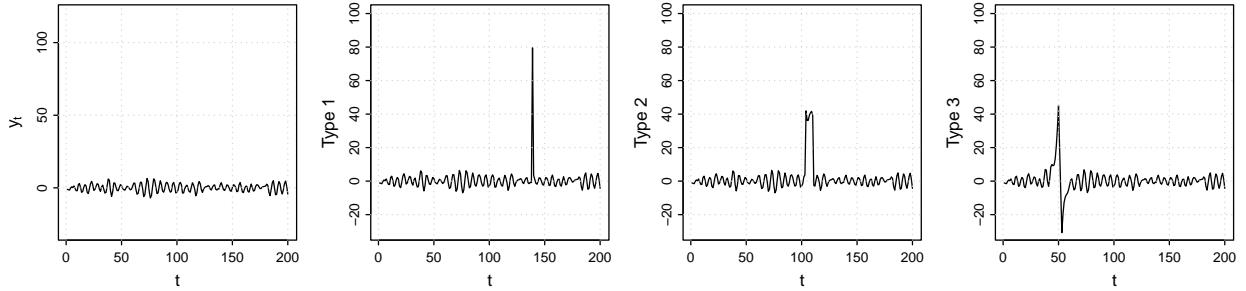


Figure 3: Time series and outlier-contaminated signals. Left to right: $y_t, y_{1,t}, y_{2,t}, y_{3,t}$. The sample size is $n = 200$ and $(c_1, c_2, c_3) = (30, 15, 15)$ times the sample standard deviation of the time series.

standard deviation of the time series, corresponding to the probabilities that $\Pr\{|y_t| \leq \psi\} = (0.5, 0.65, 0.82)$. Then, we compute the power of Fisher’s test and obtain the probability of detection (PD) under significance levels 0.01, 0.05. Table 1-3 list the PD values for the models 14 - 17, along with the differences (PD of y_t minus PD of $y_{i,t}, i = 1, \dots, 3$).

We observed that the periodicity can be easily detected by all types of periodograms in the absence of outliers, with all values in the top two rows of Tables 1 - 3 close to 1. But when outliers are introduced, the PD of the EP and PG decreases rapidly, resulting in large differences, while the PD of the AHP remains comparatively stable, resulting in smaller discrepancies. Figure 4 depicts the averaged periodograms of the 1,000 simulations, illustrating that the large peak disappears gradually vanishes in the EP and PG as the outlier magnitude increases, but remains large in the AHP. Notably, for model (15), both the EP and PG become nearly constant, losing all spectral features.

We also observe that as ψ increases (the EP can be viewed as a limiting case of the AHP with $\psi \rightarrow \infty$), the AHP losses robustness, but gains computational efficiency. Specifically, the averaged estimation time of different values of ψ are reported at the bottom of Table 1. All computations were performed on a PC equipped with an Intel Core i9-13900KF CPU @5.2GHz using a single thread, 64 GB of RAM, and an Nvidia RTX 4090 GPU.

5 Real Data Applications

We analyze three real-world time series to demonstrate the effectiveness of the AHP in revealing hidden periodicities and its robustness against outliers.

In the first example, we examine the daily log returns of the S&P 500 Index over the period 1986–2015. As shown in Figure 5, the AHPs at $\alpha = 0.1$ and 0.9 successfully identify the approximately 10-year cyclical component of market volatility. In contrast, the PG produces a nearly featureless flat line like the AHP at $\alpha = 0.5$ (also, the HP). We further compute the AHS at $\alpha = 0.05, 0.07, \dots, 0.95$ and observe that the spectral feature is similar to the AHS of a GARCH(1,1) model (Engle, 1982; Bollerslev, 1986):

$$y_t \sim N(0, \sigma_t^2), \tag{18}$$

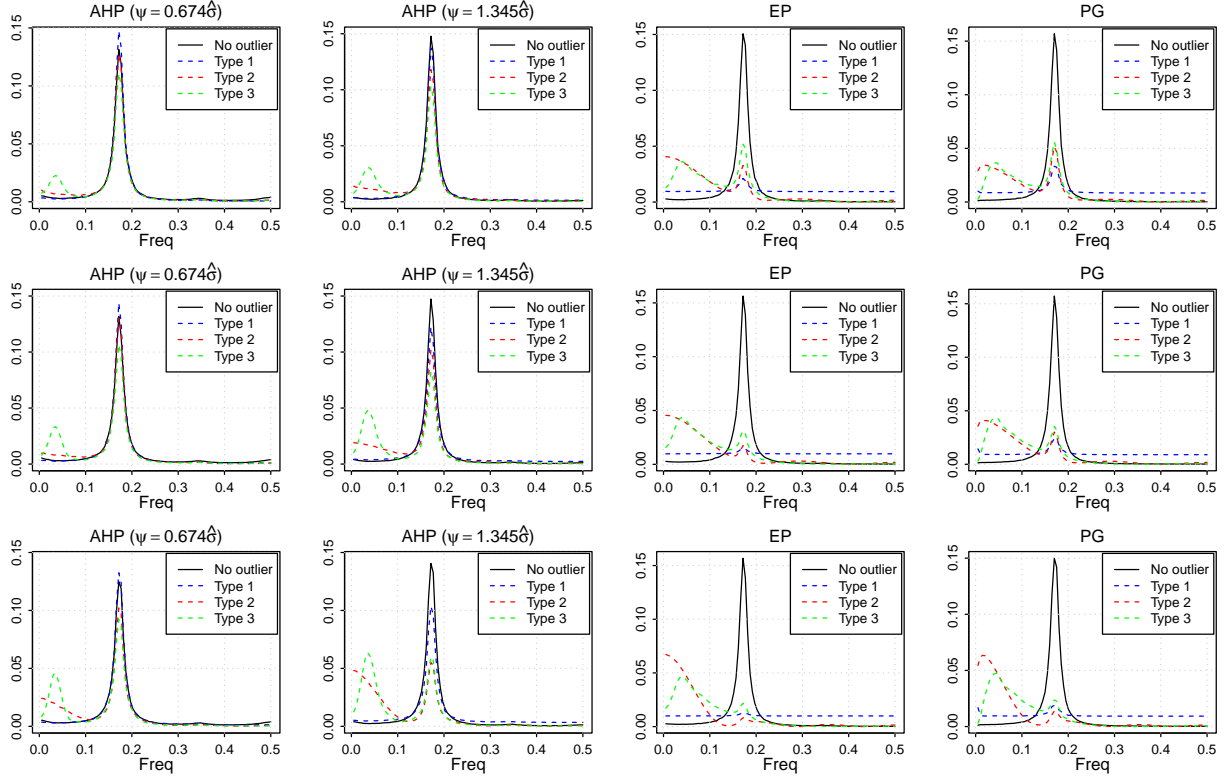


Figure 4: Left to right: the AHPs ($\alpha = 0.6, \psi = 0.674\hat{\sigma}$), the AHPs ($\alpha = 0.6, \psi = 1.345\hat{\sigma}$), the EP ($\alpha = 0.6$), and the PG, respectively. Top to bottom: (c_1, c_2, c_3) is set to $(20, 10, 10)$, $(30, 15, 15)$ and $(40, 20, 20)$, respectively. The periodograms are the average of 1,000 realizations and $n = 200$.

where $\sigma_t^2 = 10^{-6} + 0.49y_{t-1}^2 + 0.49\sigma_{t-1}^2$. The AHS captures the spectral patterns of the GARCH(1,1) model at both lower and upper α in the low frequencies, while in ordinary spectral analysis, the power spectrum is a constant. The AHS is obtained by averaging 5,000 smoothed AHPs.

The second example analyzes the epilepsy electroencephalogram (EEG) data. As illustrated in Figure 6, the PG in Figure 6 (b) identifies both low-frequency and high-frequency components, corresponding to the six main spikes and the associated bursts, respectively. However, the AHPs reveal richer structure, demonstrating that the high-frequency oscillations appear predominantly at larger α . This finding aligns well with the EEG data, where the bursts primarily occur at the top of the main spikes.

The last example analyzes the heart rate variability (HRV) data. HRV quantifies variations in heart rate over time based on electrocardiographic (ECG) record. It is represented as a time series of beat-to-beat (RR) intervals where "time" corresponds to the heartbeat index. Due to premature or skipped heartbeats, ectopic events often appear as sharp spikes in the RR tachogram (a plot of RR intervals against the beat number). Moreover, missed or inaccurate beat detection during data acquisition can introduce additional spikes. Many techniques have been proposed to eliminate

Table 1: Fisher’s test based on Type 1 outlier.

Model	Significance level	AHP ($\psi = 0.674\hat{\sigma}$)		AHP ($\psi = 0.935\hat{\sigma}$)		AHP ($\psi = 1.345\hat{\sigma}$)		EP		PG
		$\alpha = 0.6$	$\alpha = 0.8$	$\alpha = 0.6$	$\alpha = 0.8$	$\alpha = 0.6$	$\alpha = 0.8$	$\alpha = 0.6$	$\alpha = 0.8$	
y_t No outliers	0.01	0.997	0.977	0.998	0.988	1.000	0.995	1.000	1.000	1.000
	0.05	1.000	0.998	1.000	1.000	1.000	1.000	1.000	1.000	1.000
$y_{1,t}$ $c_1 = 20\hat{\sigma}$	0.01	0.999	0.989	1.000	0.994	1.000	0.994	0.380	0.015	0.641
	0.05	1.000	0.999	1.000	1.000	1.000	1.000	0.570	0.049	0.809
$y_{1,t}$ $c_1 = 30\hat{\sigma}$	0.01	1.000	0.994	1.000	0.994	1.000	0.991	0.055	0.000	0.198
	0.05	1.000	1.000	1.000	1.000	1.000	0.999	0.148	0.000	0.359
$y_{1,t}$ $c_1 = 40\hat{\sigma}$	0.01	1.000	0.994	1.000	0.993	0.999	0.982	0.004	0.000	0.037
	0.05	1.000	1.000	1.000	1.000	0.994	0.018	0.000	0.000	0.106
Difference $c_1 = 20\hat{\sigma}$	0.01	-0.002	-0.012	-0.002	-0.006	0.000	0.001	0.620	0.985	0.359
	0.05	0.000	-0.001	0.000	0.000	0.000	0.000	0.430	0.951	0.191
Difference $c_1 = 30\hat{\sigma}$	0.01	-0.003	-0.017	-0.002	-0.006	0.000	0.004	0.945	1.000	0.802
	0.05	0.000	-0.002	0.000	0.000	0.000	0.001	0.852	1.000	0.641
Difference $c_1 = 40\hat{\sigma}$	0.01	-0.003	-0.017	-0.002	-0.005	0.001	0.013	0.996	1.000	0.963
	0.05	0.000	-0.002	0.000	0.000	0.000	0.006	0.982	1.000	0.894
Time (Sec.)		0.297		0.227		0.223		0.189		

such artifacts (Acar et al., 2000; Storck et al., 2001), however, these algorithms are not entirely error-free. Therefore, we apply the AHP to explore the spectral features of the HRV data without pre-elimination of artifacts.

The data are obtained from the CAST RR Interval Sub-Study Database (file m003b) at (www.physionet.org/physiobank/database/crisdb), which provides free access to recorded physiological signals. In this application, we use the spectrogram to identify the spectral evolution of the RR intervals over time. First, we generate a moving window of length $n = 400$ beats (roughly 5 minutes) with an overlap of 200 beats (about two minutes and half). Then, we compute the AHP of the segment (in log) at fixed (α, ψ) as a function of ω , and concatenate the results to form the AHP spectrogram. Figure 7 illustrates the RR intervals and corresponding spectrograms. As can be seen, the ordinary spectrogram is completely masked whenever a spike occurs within the moving window. Moreover, when spikes occur frequently, the ordinary spectrogram fails to provide any meaningful spectral information. In contrast, the AHP spectrogram performs better, with the narrowband low-frequency component around $\omega = 0.06 \times 2\pi$ remains visible at more time. In addition, the AHP spectrogram also reveals some broadband high-frequency patterns around $\omega = 0.3 \times 2\pi$. The destructive impact of spiky contamination on the PG matches the results in Section 4.2.

6 Conclusion

We have proposed the AHP as non-parametric tool for time series analysis. The AHP offers more information than the HP by selecting the asymmetric parameter across $(0, 1)$. The threshold parameter makes the AHP a more flexible estimator in balancing robustness and efficiency. We established the asymptotic theory and investigated the relationship

Table 2: Fisher's test based on Type 2 outlier.

Model	Significance level	AHP ($\psi = 0.674\hat{\sigma}$)		AHP ($\psi = 0.935\hat{\sigma}$)		AHP ($\psi = 1.345\hat{\sigma}$)		EP		PG
		$\alpha = 0.6$	$\alpha = 0.8$	$\alpha = 0.6$	$\alpha = 0.8$	$\alpha = 0.6$	$\alpha = 0.8$	$\alpha = 0.6$	$\alpha = 0.8$	
y_t	0.01	0.997	0.977	0.998	0.988	1.000	0.995	1.000	1.000	1.000
No outliers	0.05	1.000	0.998	1.000	1.000	1.000	1.000	1.000	1.000	1.000
$y_{2,t}$	0.01	0.999	0.940	0.999	0.931	0.996	0.819	0.103	0.000	0.325
$c_2 = 10\hat{\sigma}$	0.05	1.000	0.984	1.000	0.977	1.000	0.930	0.238	0.000	0.521
$y_{2,t}$	0.01	0.999	0.932	0.996	0.836	0.976	0.491	0.000	0.000	0.012
$c_2 = 15\hat{\sigma}$	0.05	1.000	0.979	1.000	0.942	0.997	0.709	0.001	0.000	0.044
$y_{2,t}$	0.01	0.998	0.874	0.981	0.640	0.912	0.148	0.000	0.000	0.000
$c_2 = 20\hat{\sigma}$	0.05	1.000	0.956	0.999	0.813	0.973	0.315	0.000	0.000	0.000
Difference	0.01	-0.002	0.037	-0.001	0.057	0.004	0.176	0.897	1.000	0.675
$c_2 = 10\hat{\sigma}$	0.05	0.000	0.014	0.000	0.023	0.000	0.070	0.762	1.000	0.479
Difference	0.01	-0.002	0.045	0.002	0.152	0.024	0.504	1.000	1.000	0.988
$c_2 = 15\hat{\sigma}$	0.05	0.000	0.019	0.000	0.032	0.000	0.201	0.992	1.000	0.956
Difference	0.01	-0.001	0.103	0.017	0.348	0.088	0.847	1.000	1.000	1.000
$c_2 = 20\hat{\sigma}$	0.05	0.000	0.042	0.001	0.187	0.027	0.685	1.000	1.000	1.000

Table 3: Fisher's test based on Type 3 outlier.

Model	Significance level	AHP ($\psi = 0.674\hat{\sigma}$)		AHP ($\psi = 0.935\hat{\sigma}$)		AHP ($\psi = 1.345\hat{\sigma}$)		EP		PG
		$\alpha = 0.6$	$\alpha = 0.8$	$\alpha = 0.6$	$\alpha = 0.8$	$\alpha = 0.6$	$\alpha = 0.8$	$\alpha = 0.6$	$\alpha = 0.8$	
y_t	0.01	0.997	0.977	0.998	0.988	1.000	0.995	1.000	1.000	1.000
No outliers	0.05	1.000	0.998	1.000	1.000	1.000	1.000	1.000	1.000	1.000
$y_{3,t}$	0.01	0.993	0.857	0.988	0.844	0.977	0.762	0.528	0.072	0.675
$c_3 = 10\hat{\sigma}$	0.05	1.000	0.961	1.000	0.954	0.998	0.901	0.740	0.165	0.845
$y_{3,t}$	0.01	0.986	0.790	0.972	0.674	0.899	0.360	0.100	0.000	0.193
$c_3 = 15\hat{\sigma}$	0.05	1.000	0.934	0.994	0.886	0.974	0.686	0.214	0.001	0.348
$y_{3,t}$	0.01	0.970	0.653	0.907	0.425	0.700	0.110	0.006	0.000	0.033
$c_3 = 20\hat{\sigma}$	0.05	0.991	0.927	0.983	0.859	0.905	0.656	0.036	0.000	0.094
Difference	0.01	0.004	0.120	0.010	0.144	0.023	0.233	0.472	0.928	0.325
$c_3 = 10\hat{\sigma}$	0.05	0.000	0.037	0.000	0.046	0.002	0.099	0.260	0.835	0.155
Difference	0.01	0.011	0.187	0.026	0.314	0.101	0.635	0.900	1.000	0.807
$c_3 = 15\hat{\sigma}$	0.05	0.000	0.064	0.006	0.114	0.026	0.314	0.786	0.999	0.652
Difference	0.01	0.027	0.324	0.091	0.563	0.300	0.885	0.994	1.000	0.967
$c_3 = 20\hat{\sigma}$	0.05	0.009	0.071	0.017	0.141	0.095	0.344	0.964	1.000	0.906

between the AHP and what we term AHS. Simulations and three real data applications demonstrate the capability of the AHP in detecting hidden periodicities, while showing robustness against outliers.

However, the AHP is not free from limitations. First, the AHP requires an additional step in choosing the threshold parameter: when ψ approaches 0, the estimator exhibits strong robustness, whereas when ψ becomes larger, the estimator becomes computationally and statistically more efficient. One can use the suggested value in Huber (1964), or

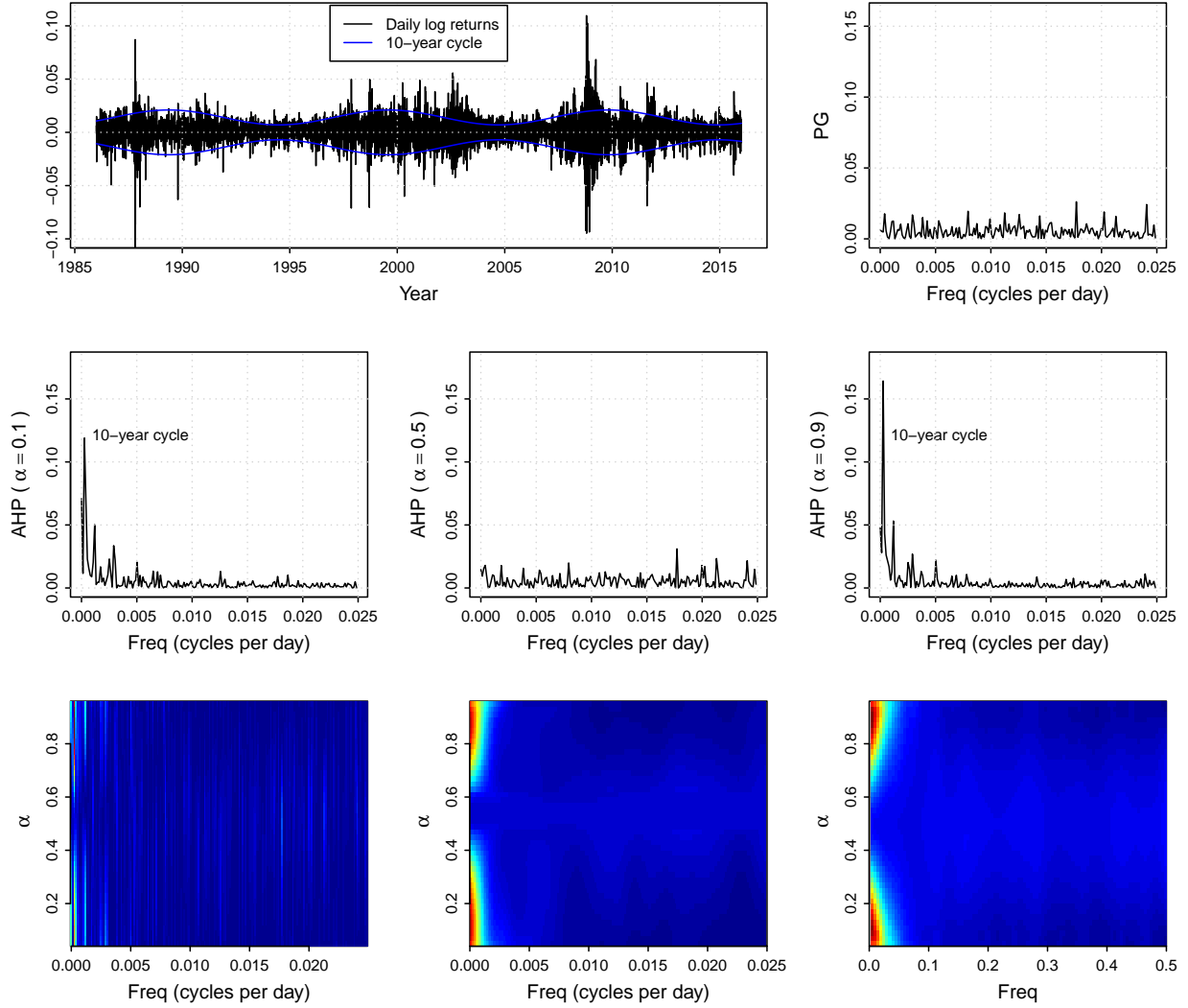


Figure 5: Top row (left): daily log returns of the S&P 500 Index data, along with its 10-year cycle; top row (right): the PG. middle row: the AHPs at $\alpha = 0.1, 0.5$ and 0.9 , respectively. Bottom row (left): the AHP at $\alpha = 0.05, 0.07, \dots, 0.95$; third row (middle): the AHS; third row (right): the AHS of model (18). The AHPs are computed at $\psi = 1.345\hat{\sigma}$

guided by the specific objectives: whether the emphasis is placed on robustness or efficiency. Second, the computational cost is much more expensive compare to the PG. The PG can be computed by the Fast Fourier Transform (FFT), while AHP is constructed using regression. Unfortunately, the computation is multiplied by the number of α . To address the computational burden, researchers can use the ordinary periodogram of $\hat{\rho}_{\alpha, \psi}(y_t - \mu(\alpha, \psi))$ to approximate the AHP. Another solution is to focus exclusively on a subset of α with sufficient discriminative power (e.g., close to 0 and 1, since when α is close to 0.5, the behavior is analogous to the PG, LP, and HP). Furthermore, we utilize multi-thread parallelization to speed up computation using the packages `foreach`, `doParallel` in R.

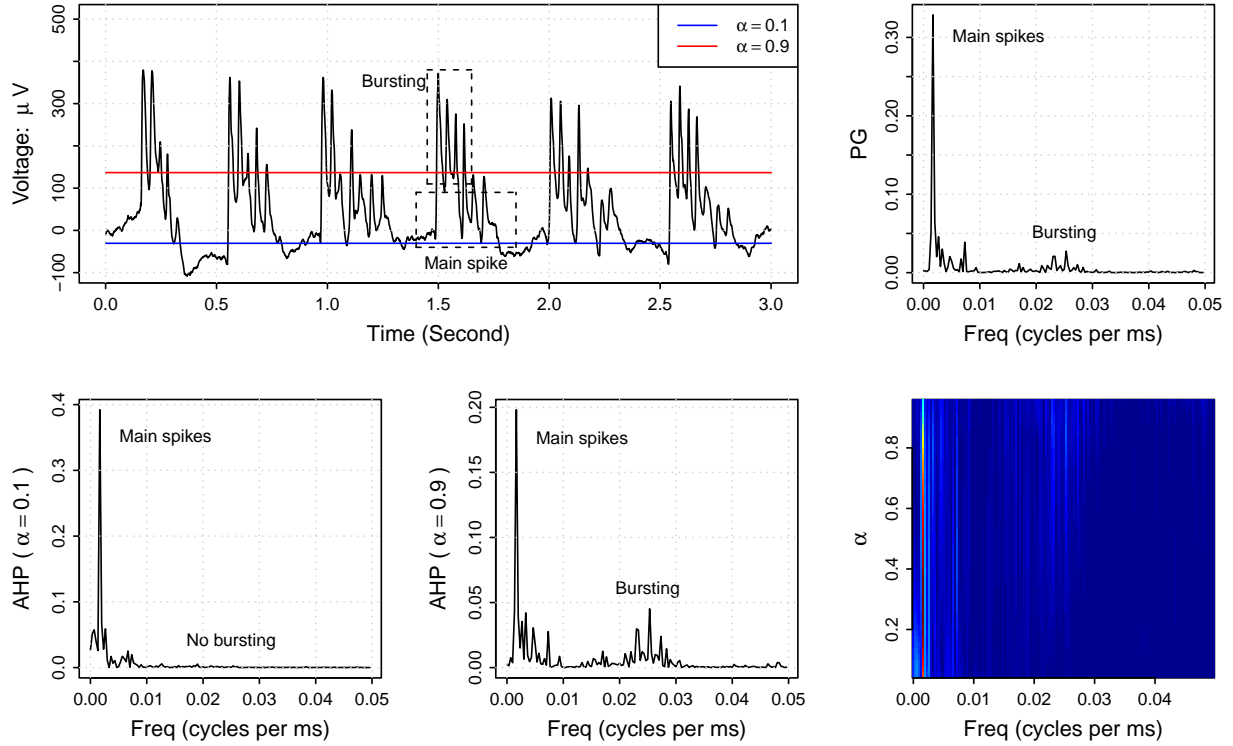


Figure 6: Top row (left): the EEG data over a 3-second interval, along with its sample expectiles; top row (right): the PG. Bottom row (left): the AHP at $\alpha = 0.1$; bottom row (middle): the AHP at $\alpha = 0.9$; bottom row (right): the AHP at $\alpha = 0.05, 0.07, \dots, 0.95$. The AHPs are computed at $\psi = 1.345\hat{\sigma}$

Further developments are needed. First, it is worthwhile to develop another type of AHP using the same way to develop type II QP in Li (2012b). Second, we can develop the joint asymptotic distribution of the AHP at different α to better understand the behavior of the AHP. Finally, developing smoothing algorithms for the AHP would enhance its practical utility, since the AHP is a rough estimator like the PG.

Acknowledgment

The authors thanks Prof. Biao Han from School of Psychology at South China Normal University for sharing the EEG data.

Funding

This work was supported by the National Natural Science Foundation of China under Grant No.12301326; Natural Science Foundation of Anhui Province under Grant No.2308085QA05; the University Natural Science Research Project of Anhui Province under Grant No.2023AH050099.

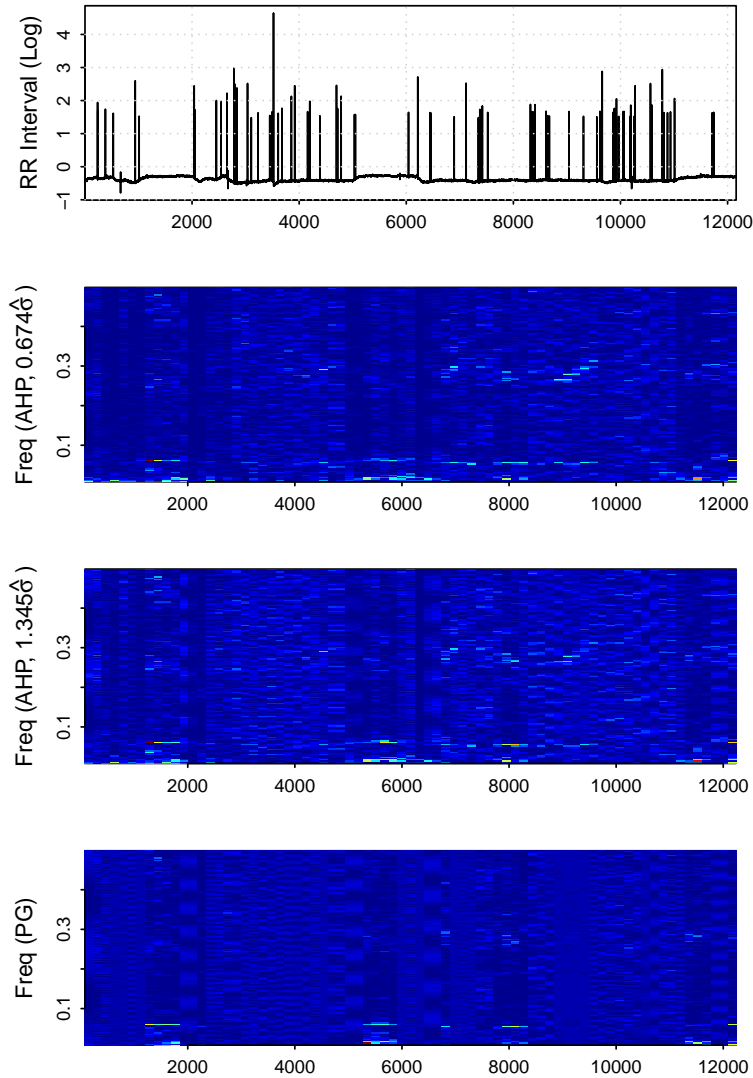


Figure 7: First row: RR tachogram (in log of a second). Second row: the AHP spectrogram at $\alpha = 0.8, \psi = 0.674\hat{\sigma}$. Third row: the AHP spectrogram at $\alpha = 0.8, \psi = 1.345\hat{\sigma}$. Fourth row: the ordinary spectrogram.

Data availability

The R code to reproduce the results, including all functions used in this paper, is available at <https://github.com/tianbochen1/K-th-Power-Expectile-Periodogram>.

References

Abo-Zahhad, M., Ahmed, S. M., and Abbas, S. N. (2015). A new eeg acquisition protocol for biometric identification using eye blinking signals. *International Journal of Intelligent Systems and Applications*, 7(6):48.

- Acar, B., Savelieva, I., Hemingway, H., and Malik, M. (2000). Automatic ectopic beat elimination in short-term heart rate variability measurement. *Computer methods and programs in biomedicine*, 63(2):123–131.
- Ahdesmäki, M., Lähdesmäki, H., Gracey, A., Shmulevich, I., and Yli-Harja, O. (2007). Robust regression for periodicity detection in non-uniformly sampled time-course gene expression data. *BMC bioinformatics*, 8(1):233.
- Albrecht, P. and Cohen, R. J. (1988). Estimation of heart rate power spectrum bands from real-world data: dealing with ectopic beats and noisy data. In *Proceedings. Computers in Cardiology 1988*, pages 311–314. IEEE.
- Allende, H., Frery, A. C., Galbiati, J., and Pizarro, L. (2006). M-estimators with asymmetric influence functions: the distribution case. *Journal of Statistical Computation and Simulation*, 76(11):941–956.
- Alvarado, R., Tillaguango, B., Dagar, V., Ahmad, M., Işık, C., Méndez, P., and Toledo, E. (2021). Ecological footprint, economic complexity and natural resources rents in latin america: empirical evidence using quantile regressions. *Journal of Cleaner Production*, 318:128585.
- Baud, M. O., Kleen, J. K., Mirro, E. A., Andrechak, J. C., King-Stephens, D., Chang, E. F., and Rao, V. R. (2018). Multi-day rhythms modulate seizure risk in epilepsy. *Nature communications*, 9(1):88.
- Bellini, F. and Di Bernardino, E. (2017). Risk management with expectiles. *The European Journal of Finance*, 23(6):487–506.
- Billingsley, P. (1995). Probability and measure. *John Wiley and Sons*.
- Birr, S., Volgushev, S., Kley, T., Dette, H., and Hallin, M. (2017). Quantile spectral analysis for locally stationary time series. *Journal of the Royal Statistical Society: Series B (Statistical Methodology)*, 79(5):1619–1643.
- Bloomfield, P. (2004). *Fourier analysis of time series: an introduction*. John Wiley & Sons.
- Bollerslev, T. (1986). Generalized autoregressive conditional heteroskedasticity. *Journal of econometrics*, 31(3):307–327.
- Brockwell, P. J. and Davis, R. A. (1991). *Time Series: Theory and Methods*. Springer.
- Cai, Z. and Xiao, Z. (2012). Semiparametric quantile regression estimation in dynamic models with partially varying coefficients. *Journal of Econometrics*, 167(2):413–425.
- Cai, Z. and Xu, X. (2008). Nonparametric quantile estimations for dynamic smooth coefficient models. *Journal of the American Statistical Association*, 103(484):1595–1608.
- Caiado, J., Crato, N., and Peña, D. (2006). A periodogram-based metric for time series classification. *Computational Statistics & Data Analysis*, 50(10):2668–2684.
- Chen, T. (2024). Expectile periodograms. *arXiv preprint arXiv:2403.02060*.
- Chen, T. (2025). Robust functional ward’s linkages with applications in eeg data clustering. *arXiv preprint arXiv:2501.11081*.

- Chen, T., Sun, Y., Euan, C., and Ombao, H. (2021a). Clustering brain signals: A robust approach using functional data ranking. *Journal of Classification*, 38:425–442.
- Chen, T., Sun, Y., and Li, T.-H. (2021b). A semi-parametric estimation method for the quantile spectrum with an application to earthquake classification using convolutional neural network. *Computational Statistics & Data Analysis*, 154:107069.
- Daouia, A., Girard, S., and Stupfler, G. (2018). Estimation of tail risk based on extreme expectiles. *Journal of the Royal Statistical Society Series B: Statistical Methodology*, 80(2):263–292.
- Dette, H., Hallin, M., Kley, T., Volgushev, S., et al. (2015). Of copulas, quantiles, ranks and spectra: An l_1 -approach to spectral analysis. *Bernoulli*, 21(2):781–831.
- Efron, B. (1991). Regression percentiles using asymmetric squared error loss. *Statistica Sinica*, pages 93–125.
- Engle, R. F. (1982). Autoregressive conditional heteroscedasticity with estimates of the variance of united kingdom inflation. *Econometrica: Journal of the Econometric Society*, 50(4):987–1007.
- Euán, C., Ombao, H., and Ortega, J. (2018). The hierarchical spectral merger algorithm: a new time series clustering procedure. *Journal of Classification*, 35:71–99.
- García, J., Hernández, P. J., and Lopez-Nicolas, A. (2001). How wide is the gap? an investigation of gender wage differences using quantile regression. *Empirical economics*, 26:149–167.
- Gu, Y. and Zou, H. (2016). High-dimensional generalizations of asymmetric least squares regression and their applications.
- Gupta, D., Hazarika, B. B., and Berlin, M. (2020). Robust regularized extreme learning machine with asymmetric huber loss function. *Neural Computing and Applications*, 32(16):12971–12998.
- Hagemann, A. (2013). Robust spectral analysis.
- Hazarika, B. B., Gupta, D., and Borah, P. (2023). Robust support vector quantile regression with truncated pinball loss (rsvqr). *Computational and Applied Mathematics*, 42(6):283.
- Huber, P. J. (1964). Robust estimation of a location parameter. *The Annals of Mathematical Statistics*, pages 73–101.
- Jiang, C., Jiang, M., Xu, Q., and Huang, X. (2017). Expectile regression neural network model with applications. *Neurocomputing*, 247:73–86.
- Jiang, Y., Lin, F., and Zhou, Y. (2021). The k th power expectile regression. *Annals of the Institute of Statistical Mathematics*, 73:83–113.
- Jones, M. C. (1994). Expectiles and m -quantiles are quantiles. *Statistics & Probability Letters*, 20(2):149–153.
- Kley, T. (2016). Quantile-based spectral analysis in an object-oriented framework and a reference implementation in R: The quantspec package. *Journal of Statistical Software, Articles*, 70(3):1–27.
- Koenker, R. (2017). Quantile regression: 40 years on. *Annual review of economics*, 9:155–176.

- Koenker, R. and Bassett Jr, G. (1978). Regression quantiles. *Econometrica: journal of the Econometric Society*, pages 33–50.
- Kouretas, G. P., Zarangas, L., et al. (2005). Conditional autoregressive value at risk by regression quantiles: Estimating market risk for major stock markets. Technical report.
- Li, T.-H. (2008). Laplace periodogram for time series analysis. *Journal of the American Statistical Association*, 103(482):757–768.
- Li, T.-H. (2012a). Detection and estimation of hidden periodicity in asymmetric noise by using quantile periodogram. In *Proceedings of the IEEE International Conference on Acoustics, Speech and Signal Processing (ICASSP)*, vol 2, pp. 3969-3972.
- Li, T.-H. (2012b). Quantile periodograms. *Journal of the American Statistical Association*, 107(498):765–776.
- Li, T.-H. (2014). Quantile periodogram and time-dependent variance. *Journal of Time Series Analysis*, 35(4):322–340.
- Li, T.-H. (2023). Quantile-frequency analysis and deep learning for signal classification. *Journal of Nondestructive Evaluation*, 42(2):40.
- Maadooliat, M., Sun, Y., and Chen, T. (2018). Nonparametric collective spectral density estimation with an application to clustering the brain signals. *To appear in Statistics in Medicine*.
- Machado, J. A. and Mata, J. (2005). Counterfactual decomposition of changes in wage distributions using quantile regression. *Journal of applied Econometrics*, 20(4):445–465.
- Malik, M. (1996). Heart rate variability: Standards of measurement, physiological interpretation, and clinical use: Task force of the european society of cardiology and the north american society for pacing and electrophysiology. *Annals of Noninvasive Electrocardiology*, 1(2):151–181.
- Mansor, W., Abd Rani, M. S., and Wahy, N. (2011). *Integrating neural signal and embedded system for controlling small motor*. InTech.
- Martínez-Murcia, F. J., Ortiz, A., Morales-Ortega, R., López, P., Luque, J. L., Castillo-Barnes, D., Segovia, F., Illan, I. A., Ortega, J., Ramirez, J., et al. (2019). Periodogram connectivity of eeg signals for the detection of dyslexia. In *Understanding the Brain Function and Emotions: 8th International Work-Conference on the Interplay Between Natural and Artificial Computation, IWINAC 2019, Almería, Spain, June 3–7, 2019, Proceedings, Part I 8*, pages 350–359. Springer.
- Meziani, A., Medkour, T., and Djouani, K. (2020). Penalised quantile periodogram for spectral estimation. *Journal of Statistical Planning and Inference*, 207:86–98.
- Newey, W. K. and Powell, J. L. (1987). Asymmetric least squares estimation and testing. *Econometrica: Journal of the Econometric Society*, pages 819–847.
- Oh, H.-S., Nychka, D., Brown, T., and Charbonneau, P. (2004). Period analysis of variable stars by robust smoothing. *Journal of the Royal Statistical Society Series C: Applied Statistics*, 53(1):15–30.

- Polat, K. and Güneş, S. (2007). Classification of epileptiform eeg using a hybrid system based on decision tree classifier and fast fourier transform. *Applied Mathematics and Computation*, 187(2):1017–1026.
- Rousseeuw, P. and Yohai, V. (1984). Robust regression by means of s-estimators. In *Robust and nonlinear time series analysis: Proceedings of a Workshop Organized by the Sonderforschungsbereich 123 “Stochastische Mathematische Modelle”, Heidelberg 1983*, pages 256–272. Springer.
- Sharif, A., Bhattacharya, M., Afshan, S., and Shahbaz, M. (2021). Disaggregated renewable energy sources in mitigating co2 emissions: new evidence from the usa using quantile regressions. *Environmental Science and Pollution Research*, 28(41):57582–57601.
- Storck, N., Ericson, M., Lindblad, L., and Jensen-Urstad, M. (2001). Automatic computerized analysis of heart rate variability with digital filtering of ectopic beats. *Clinical Physiology*, 21(1):15–24.
- Thieler, A. M. (2014). Robuste verfahren zur periodendetektion in ungleichmäßig beobachteten lichtkurven.
- Thieler, A. M., Fried, R., and Rathjens, J. (2016). Robper: An r package to calculate periodograms for light curves based on robust regression. *Journal of Statistical Software*, 69:1–37.
- Waltrup, L. S., Sobotka, F., Kneib, T., and Kauermann, G. (2015). Expectile and quantile regression—david and goliath? *Statistical Modelling*, 15(5):433–456.
- Wen, Q., He, K., Sun, L., Zhang, Y., Ke, M., and Xu, H. (2021). Robustperiod: Robust time-frequency mining for multiple periodicity detection. In *Proceedings of the 2021 international conference on management of data*, pages 2328–2337.
- Xu, Q., Chen, L., Jiang, C., and Yu, K. (2020). Mixed data sampling expectile regression with applications to measuring financial risk. *Economic Modelling*, 91:469–486.
- Xu, Q., Ding, X., Jiang, C., Yu, K., and Shi, L. (2021). An elastic-net penalized expectile regression with applications. *Journal of Applied Statistics*, 48(12):2205–2230.
- Yao, Q. and Tong, H. (1996). Asymmetric least squares regression estimation: a nonparametric approach. *Journal of nonparametric statistics*, 6(2-3):273–292.
- Ziegel, J. F. (2016). Coherence and elicibility. *Mathematical Finance*, 26(4):901–918.

Appendix A

A.1 Lemma and Proof

Let the following assumptions be satisfied:

- A1. The cumulative distribution function $F(\cdot)$ is Lipschitz continuous, i.e., there exists a constant $K > 0$ such that $|F(y) - F(y')| \leq K|y - y'|$ for all $y, y' \in \mathbb{R}$.

A2. The regressor sequence $\{\mathbf{x}_{nt}\}$ is bounded with finite moments $\sup_{n,t} \|\mathbf{x}_{nt}\| \leq C_x < \infty$ and $\sup_t E\|\mathbf{x}_{nt}\|^4 < \infty$.

A3. The process $\{y_t\}$ has the strong mixing property with mixing numbers a_τ ($\tau = 1, 2, \dots$) satisfying $a_\tau \rightarrow 0$ as $\tau \rightarrow \infty$.

A4. There exists a positive definite matrix \mathbf{D}_j for all j such that $\mathbf{D}_{jn} \rightarrow \mathbf{D}_j$ as $n \rightarrow \infty$, where

$$\mathbf{D}_{jn} := n^{-1} \sum_{t=1}^n \mathbf{x}_{jnt} \mathbf{x}_{jnt}^\top.$$

A5. There exists a positive definite matrix $\mathbf{V}_{jl}(\alpha, \psi)$ for all j, l such that $\mathbf{V}_{jln}(\alpha, \psi) \rightarrow \mathbf{V}_{jl}(\alpha, \psi)$ as $n \rightarrow \infty$, where

$$\mathbf{V}_{jln}(\alpha, \psi) := n^{-1} \sum_{t=1}^n \sum_{s=1}^n \text{Cov}\{\dot{\rho}_{\alpha, \psi}(y_t - \mu(\alpha, \psi)), \dot{\rho}_{\alpha, \psi}(y_s - \mu(\alpha, \psi))\} \mathbf{x}_{jnt} \mathbf{x}_{jns}^\top, \quad j, l = 1, \dots, q. \quad (19)$$

A6. A central limit theorem is valid for $\text{vec}[\zeta_{jn}(\alpha, \psi)]_{j=1}^q$ for all j , i.e., $\text{vec}[\zeta_{jn}(\alpha, \psi)]_{j=1}^q \xrightarrow{D} N(\mathbf{0}, [\mathbf{V}_{jl}(\alpha, \psi)]_{j,l=1}^q)$ as $n \rightarrow \infty$.

Lemma 1 (Asymmetric Huber Regression). If (A1) - (A6) are satisfied, then

$$\sqrt{n} \text{vec}[\hat{\boldsymbol{\beta}}_{jn}(\alpha, \psi) - \boldsymbol{\beta}_0(\alpha, \psi)]_{j=1}^q \xrightarrow{D} N(\mathbf{0}, [\boldsymbol{\Lambda}_j^{-1}(\alpha, \psi) \mathbf{V}_{jl}(\alpha, \psi) \boldsymbol{\Lambda}_l^{-1}(\alpha, \psi)]_{j,l=1}^q),$$

where

$$\hat{\boldsymbol{\beta}}_{jn}(\alpha, \psi) := \arg \min_{\boldsymbol{\beta}_j \in \mathbb{R}^p} \sum_{t=1}^n \rho_{\alpha, \psi}(y_t - \mathbf{x}_{jnt}^\top \boldsymbol{\beta}_j),$$

$\boldsymbol{\beta}_0(\alpha, \psi) := [\mu(\alpha, \psi), 0, \dots, 0]^\top \in \mathbb{R}^p$, and

$$\boldsymbol{\Lambda}_j(\alpha, \psi) := \lim_{n \rightarrow \infty} \boldsymbol{\Lambda}_{jn}(\alpha, \psi) := \lim_{n \rightarrow \infty} \eta^{-1}(\alpha, \psi) \mathbf{D}_{jn} = \eta^{-1}(\alpha, \psi) \mathbf{D}_j.$$

Proof. First, consider the case of $q = 1$ for which we drop the subscript j in the notation for simplicity. Let $U_t := y_t - \mu(\alpha, \psi) = y_t - \mathbf{x}_{nt}^\top \boldsymbol{\beta}_0(\alpha, \psi)$ and $c_{nt}(\boldsymbol{\delta}) := n^{-1/2} \mathbf{x}_{nt}^\top \boldsymbol{\delta}$ with $\boldsymbol{\delta} \in \mathbb{R}^p$, consider the random function

$$Z_n(\boldsymbol{\delta}) := \sum_{t=1}^n \{\rho_{\alpha, \psi}(U_t - c_{nt}(\boldsymbol{\delta})) - \rho_{\alpha, \psi}(U_t)\}.$$

Note that by reparameterizing $\boldsymbol{\delta} := \sqrt{n}(\boldsymbol{\beta} - \boldsymbol{\beta}_0(\alpha, \psi))$ as a function of $\boldsymbol{\beta} \in \mathbb{R}^p$, one can write

$$Z_n(\boldsymbol{\delta}) = \sum_{t=1}^n \{\rho_{\alpha, \psi}(y_t - \mathbf{x}_{nt}^\top \boldsymbol{\beta}) - \rho_{\alpha, \psi}(U_t)\}.$$

Therefore, the minimizer of $Z_n(\boldsymbol{\delta})$ over $\boldsymbol{\delta} \in \mathbb{R}^p$ takes the form

$$\hat{\boldsymbol{\delta}}_n := \arg \min_{\boldsymbol{\delta} \in \mathbb{R}^p} Z_n(\boldsymbol{\delta}) = \sqrt{n}(\hat{\boldsymbol{\beta}}_n(\alpha, \psi) - \boldsymbol{\beta}_0(\alpha, \psi)).$$

We aim to prove

$$\hat{\boldsymbol{\delta}}_n = \boldsymbol{\Lambda}_n^{-1} \boldsymbol{\zeta}_n + o_P(1). \quad (20)$$

Here we drop the argument α, ψ from $\boldsymbol{\Lambda}_n$ and $\boldsymbol{\zeta}_n$ for simplicity of notation, as α and ψ are fixed numbers. In order to arrive at (20), we first would like to prove that

$$Z_n(\boldsymbol{\delta}) = \tilde{Z}_n(\boldsymbol{\delta}) + o_P(1), \quad (21)$$

for any fixed δ , where $\tilde{Z}_n(\delta) := -\delta^T \zeta_n + (1/2)\delta^T \Lambda_n \delta$. If (21) holds, then, due to the convexity of $Z_n(\delta)$ and $\tilde{Z}_n(\delta)$ as functions of δ , one can follow the argument of Li (2008) to show that $\hat{\delta}_n$ as the minimizer of $Z_n(\delta)$ is $o_P(1)$ away from the minimizer of $\tilde{Z}_n(\delta)$, which equals $\Lambda_n^{-1} \zeta_n$. This completes the proof of (20).

Using Taylor formula, we have

$$\rho_{\alpha, \psi}(U_t - c_{nt}) - \rho_{\alpha, \psi}(U_t) = -c_{nt} \dot{\rho}_{\alpha, \psi}(U_t) + \frac{1}{2} c_{nt}^2 \ddot{\rho}_{\alpha, \psi}(U_t) + R_{nt}.$$

Here, we drop the argument δ from R_{nt} and c_{nt} for simplicity of notation as δ is fixed in the remainder of the proof. Then,

$$Z_n(\delta) = -\delta^T \zeta_n + \delta^T \Lambda_n \delta + \sum_{t=1}^n R_{nt},$$

and (21) is equivalent to

$$\sum_{t=1}^n R_{nt} = o_P(1). \quad (22)$$

And (22) can be established by proving that

$$\mathbb{E} \left\{ \sum_{t=1}^n R_{nt} \right\} = o(1), \quad (23)$$

and

$$\text{Var} \left\{ \sum_{t=1}^n R_{nt} \right\} = o(1). \quad (24)$$

When U_t and $U_t - c_{nt}$ lie in $|u| \leq \psi$ or $|u| > \psi$, R_{nt} is $O(c_{nt}^3)$ because $\ddot{\rho}$ is constant in the same segment of ρ . We focus on R_{nt} if $(U_t - c_{nt}, U_t)$ crosses one of $\{-\psi, 0, \psi\}$. Define the crossing event

$$\mathcal{C}_t := \{U_t \text{ and } U_t - c_{nt} \text{ lie in different segments across } \{-\psi, 0, \psi\}\}.$$

Whenever a crossing occurs (i.e. \mathcal{C}_t holds),

$$|R_{nt}| \leq C_{\alpha, \psi} c_{nt}^2 I(\mathcal{C}_t),$$

for some $C_{\alpha, \psi} > 0$ depending only on (α, ψ) . Using (A2), $|c_{nt}| \leq n^{-1/2} C_x \|\delta\|$, hence

$$|R_{nt}| \leq \kappa n^{-1}, \quad (25)$$

where $\kappa := C_{\alpha, \psi} C_x^2 \|\delta\|^2$. Then,

$$\mathbb{E}|R_{nt}| \leq C_{\alpha, \psi} \mathbb{E} \{c_{nt}^2 I(\mathcal{C}_t)\}.$$

By Cauchy–Schwarz,

$$\mathbb{E} \{c_{nt}^2 I(\mathcal{C}_t)\} \leq \sqrt{\mathbb{E}(c_{nt}^4)} \cdot \sqrt{\Pr(\mathcal{C}_t)}.$$

Using $c_{nt} = n^{-1/2} \mathbf{x}_{nt}^\top \delta$ with (A2),

$$\mathbb{E}\{c_{nt}^4\} = n^{-2} \mathbb{E}\{(\mathbf{x}_{nt}^\top \delta)^4\} \leq n^{-2} C_x^4 \|\delta\|^4 = O(n^{-2}).$$

By (A1) the crossing probability satisfies

$$\Pr(\mathcal{C}_t) \leq L|c_{nt}| = O(n^{-1/2}),$$

uniformly in t . Combining yields

$$E \{ c_{nt}^2 I(\mathcal{C}_t) \} = O(n^{-2})^{1/2} \cdot O(n^{-1/2})^{1/2} = O(n^{-1} \cdot n^{-1/4}) = O(n^{-5/4}).$$

Hence

$$E \left\{ \sum_{t=1}^n R_{nt} \right\} = o(1).$$

Furthermore, for any $0 < m < n$, we split the variance in (24) into two terms:

$$\text{Var} \left\{ \sum_{t=1}^n R_{nt} \right\} = \left(\sum_{(t,s) \in D_m} + \sum_{(t,s) \in D'_m} \right) \text{Cov}(R_{nt}, R_{ns}), \quad (26)$$

where $D_m := \{(t, s) : |t - s| \leq m, 1 \leq t, s \leq n\}$ and $D'_m := \{(t, s) : |t - s| > m, 1 \leq t, s \leq n\}$. The expression (24) is obtained if both terms in (26) can be shown to take the form $o(1)$. Then

$$\text{Var} \left(\sum_{t=1}^n R_{nt} \right) = \sum_{(t,s) \in D_m} \text{Cov}(R_{nt}, R_{ns}) + \sum_{(t,s) \in D'_m} \text{Cov}(R_{nt}, R_{ns}).$$

For $(t, s) \in D_m$, use (25) to get

$$\text{Var}\{R_{nt}\} \leq E\{R_{nt}^2\} \leq \kappa^2 n^{-2},$$

which implies that

$$|\text{Cov}(R_{nt}, R_{ns})| \leq \sqrt{\text{Var}\{R_{nt}\} \text{Var}\{R_{ns}\}} \leq \kappa^2 n^{-2}. \quad (27)$$

Observe that the number of elements in D_m is bounded above by $(2m + 1)n$. Combining this result with (27) yields

$$\left| \sum_{(t,s) \in D_m} \text{Cov}(R_{nt}, R_{ns}) \right| \leq |D_m| \cdot (\kappa n^{-1})^2 \leq (2m + 1)n \cdot \kappa^2 n^{-2} = (2m + 1)\kappa^2 n^{-1}. \quad (28)$$

For $(t, s) \in D'_m$, $\{U_t\}$ is a stationary process with the same strong mixing property as $\{y_t\}$ under assumption (A4). Because R_{nt} is a function of U_t and R_{ns} is a function of U_s , both bounded by κn^{-1} according to (25), citing the mixing inequality (Billingsley, 1995) yields:

$$|\text{Cov}(R_{nt}, R_{ns})| \leq 4 \|R_{nt}\|_\infty \|R_{ns}\|_\infty a_{|t-s|} \leq 4\kappa^2 n^{-2} a_{|t-s|}.$$

Therefore, we have

$$\begin{aligned} \left| \sum_{(t,s) \in D'_m} \text{Cov}(R_{nt}, R_{ns}) \right| &\leq \sum_{m < |\tau| < n, 1 \leq s \leq n} |\text{Cov}(R_{n, s+\tau}, R_{ns})| \\ &\leq \sum_{m < |\tau| < n} n \times 4\kappa^2 n^{-2} a_{|\tau|} \\ &\leq 8\kappa^2 n^{-1} \sum_{\tau=m+1}^n a_\tau \\ &= 8\kappa^2 \left\{ n^{-1} \sum_{\tau=1}^n a_\tau - (m/n) m^{-1} \sum_{\tau=1}^m a_\tau \right\}. \end{aligned} \quad (29)$$

Choose $m = m_n \rightarrow \infty$ with $m_n/n \rightarrow 0$. Because $a_\tau \rightarrow 0$ as $\tau \rightarrow \infty$, it follows from the Stolz-Cesàro theorem that $n^{-1} \sum_{\tau=1}^n a_\tau \rightarrow 0$ as $n \rightarrow \infty$ and $m^{-1} \sum_{\tau=1}^m a_\tau \rightarrow 0$ as $m \rightarrow \infty$. In this case, (28) and (29) imply

$$\sum_{(t,s) \in D_m} \text{Cov}(R_{nt}, R_{ns}) = o(1) \quad \text{and} \quad \sum_{(t,s) \in D'_m} \text{Cov}(R_{nt}, R_{ns}) = o(1), \quad (30)$$

separately. Then, we reach (24). Combining (23) and (24) prove (22), which implies

$$\sqrt{n}(\hat{\beta}_n(\alpha) - \beta_0(\alpha)) = \mathbf{\Lambda}_n^{-1}(\alpha) \zeta_n(\alpha) + o_P(1). \quad (31)$$

Next, we would like to establish the asymptotic normality of the AHR solution. Because $\mu(\alpha, \psi)$ satisfies (2), it follows that

$$\mathbf{E}\{\zeta_n(\alpha, \psi)\} = n^{-1/2} \sum_{t=1}^n \mathbf{E}\{\dot{\rho}_{\alpha, \psi}(y_t - \mu(\alpha, \psi))\} \mathbf{x}_{nt} = \mathbf{0}.$$

Moreover, we have

$$\mathbf{V}_n(\alpha, \psi) := \text{Cov}\{\zeta_n(\alpha, \psi)\} = n^{-1} \sum_{t=1}^n \sum_{s=1}^n \text{Cov}\{\dot{\rho}_{\alpha, \psi}(y_t - \mu(\alpha, \psi)), \dot{\rho}_{\alpha, \psi}(y_s - \mu(\alpha, \psi))\} \mathbf{x}_{nt} \mathbf{x}_{ns}^\top.$$

Then, collecting assumptions (A5)-(A7) and (31), we obtain

$$\mathbf{\Lambda}_n(\alpha, \psi)^{-1} \zeta_n(\alpha, \psi) \xrightarrow{D} N(\mathbf{0}, \mathbf{\Lambda}^{-1}(\alpha, \psi) \mathbf{V}(\alpha, \psi) \mathbf{\Lambda}^{-1}(\alpha, \psi)).$$

For the general case of $q > 1$, we re-add the subscript j in the notation. Citing results in Li (2008) and Chen (2024), we obtain the general case of $q > 1$. Then, **Lemma 1** is proved.

A.2 Proof of Theorem 1

For fixed $q > 1$ and $0 < \lambda_1 < \dots < \lambda_q < \pi$, let $\omega_{\nu_1}, \dots, \omega_{\nu_q}$ be Fourier frequencies satisfying $\omega_{\nu_j} \rightarrow \lambda_j$ as $n \rightarrow \infty$ for $j = 1, \dots, q$. The trigonometric regressor $\mathbf{x}_{jnt} := [\cos(\omega_{\nu_j} t), \sin(\omega_{\nu_j} t)]^\top$ is bounded, so (A2) is satisfied. It is easy to verify that when $n \rightarrow \infty$,

$$\mathbf{D}_{jn} = n^{-1} \sum_{t=1}^n \mathbf{x}_{jt}(\omega_{\nu_j}) \mathbf{x}_{jt}^\top(\omega_{\nu_j}) \rightarrow \mathbf{D}_j = \text{diag}\{1/2, 1/2\},$$

so (A5) is satisfied. It follows from (19) that, when $j = k$,

$$\mathbf{V}_{jjn}(\alpha, \psi) = \sum_{|\tau| < n} \gamma(\tau, \alpha, \psi) \left\{ n^{-1} \sum_{t=\max(1, 1+\tau)}^{\min(n, n+\tau)} \mathbf{x}_{jt}(\omega_{\nu_j}) \mathbf{x}_{j, t-\tau}^\top(\omega_{\nu_j}) \right\}.$$

For fixed τ , we have

$$n^{-1} \sum_{t=\max(1, 1+\tau)}^{\min(n, n+\tau)} \mathbf{x}_{jt}(\omega_{\nu_j}) \mathbf{x}_{j, t-\tau}^\top(\omega_{\nu_j}) \rightarrow (1/2) \mathbf{S}(\lambda_j),$$

where

$$\mathbf{S}(\lambda_j) := \begin{bmatrix} \cos(\lambda_j \tau) & -\sin(\lambda_j \tau) \\ \sin(\lambda_j \tau) & \cos(\lambda_j \tau) \end{bmatrix}.$$

Then,

$$\begin{aligned}
\mathbf{V}_{jj}(\alpha, \psi) &:= \lim_{n \rightarrow \infty} \mathbf{V}_{jjn}(\alpha, \psi) \\
&= \sum_{\tau=-\infty}^{\infty} \gamma(\tau, \alpha, \psi) (1/2) \mathbf{S}(\lambda_j) \\
&= \text{diag}\{(1/2)h(\lambda_j, \alpha, \psi), (1/2)h(\lambda_j, \alpha, \psi)\}.
\end{aligned} \tag{32}$$

When $j \neq l$,

$$\mathbf{V}_{jl}(\alpha, \psi) := \lim_{n \rightarrow \infty} \mathbf{V}_{jln}(\alpha, \psi) = \mathbf{0}. \tag{33}$$

Based on (32) and (33), we have

$$\mathbf{V}_{jl}(\alpha, \psi) = \delta_{j-l} \text{diag}\{(1/2)h(\lambda_j, \alpha, \psi), (1/2)h(\lambda_j, \alpha, \psi)\},$$

where δ_s denotes the Kronecker delta function, and

$$[\mathbf{\Lambda}_j^{-1}(\alpha, \psi) \mathbf{V}_{jl}(\alpha, \psi) \mathbf{\Lambda}_l^{-1}(\alpha, \psi)]_{j,l=1}^q = \text{diag}\{2g(\lambda_1, \alpha, \psi), 2g(\lambda_1, \alpha, \psi), \dots, 2g(\lambda_q, \alpha, \psi), 2g(\lambda_q, \alpha, \psi)\}.$$

Hence, (A6) is satisfied. Moreover, (C1) - (C4) repeat (A1), (A3), (A4) and (A7), respectively. Finally, all assumptions (A1)-(A7) are satisfied. Therefore, by **Lemma 1**,

$$\sqrt{n} \text{vec}[\hat{\boldsymbol{\beta}}_{jn}(\omega_{\nu_j}, \alpha, \psi) - \boldsymbol{\beta}_0(\alpha, \psi)]_{j=1}^q \xrightarrow{D} N(\mathbf{0}, \text{diag}\{2g(\lambda_1, \alpha, \psi), 2g(\lambda_1, \alpha, \psi), \dots, 2g(\lambda_q, \alpha, \psi), 2g(\lambda_q, \alpha, \psi)\})$$

Further, because $\hat{\boldsymbol{\beta}}_n(\omega_{\nu_j}, \alpha, \psi) = [\hat{\beta}_1(\omega_{\nu_j}, \alpha, \psi), \hat{\beta}_2(\omega_{\nu_j}, \alpha, \psi)]^\top$, we have

$$\sqrt{n} [\hat{\beta}_1(\omega_{\nu_j}, \alpha, \psi), \hat{\beta}_2(\omega_{\nu_j}, \alpha, \psi)]^\top / \sqrt{2g(\lambda_j, \alpha, \psi)} \xrightarrow{D} N(\mathbf{0}, \mathbf{I}),$$

and hence

$$\text{AHP}_n(\omega_{\nu_j}, \alpha, \psi) / g(\lambda_j, \alpha, \psi) = \frac{n}{4} \{\hat{\beta}_1^2(\omega_{\nu_j}, \alpha, \psi) + \hat{\beta}_2^2(\omega_{\nu_j}, \alpha, \psi)\} / g(\lambda_j, \alpha, \psi) \sim \frac{1}{2} (\xi_1^2 + \xi_2^2) = \chi_2^2,$$

where ξ_1 and ξ_2 are i.i.d. $N(0, 1)$ random variables. This implies that $\text{AHP}_n(\omega_{\nu_j}, \alpha, \psi)$ are asymptotically independent with distribution $g(\lambda_j, \alpha, \psi) (1/2) \chi_{2,j}^2$ for each j , and we obtain (10).